The Journal of Experimental Biology 210, 1897-1911
Published by The Company of Biologists 2007
doi:10.1242/jeb.002055

Low speed maneuvering flight of the rose-breasted cockatoo (*Eolophus roseicapillus*). I. Kinematic and neuromuscular control of turning

T. L. Hedrick[1,*] and A. A. Biewener[2]

[1]*Department of Biology, CB 3280 Coker Hall, University of North Carolina, Chapel Hill, NC 27599-3280, USA and*
[2]*Concord Field Station, MCZ, Harvard University, Old Causeway Road, Bedford, MA 01730, USA*

*Author for correspondence (e-mail: thedrick@bio.unc.edu)

Accepted 6 March 2007

Summary

Maneuvering flight has long been recognized as an important component of the natural behavior of many bird species, but has been the subject of little experimental work. Here we examine the kinematics and neuromuscular control of turning flight in the rose-breasted cockatoo *Eolophus roseicapillus* (*N*=6), testing predictions of maneuvering flight and control based on aerodynamic theory and prior kinematic and neuromuscular studies. Six cockatoos were trained to navigate between two perches placed in an L-shaped flight corridor, making a 90° turn midway through each flight. Flights were recorded with three synchronized high-speed video cameras placed outside the corridor, allowing a three-dimensional reconstruction of wing and body kinematics through the turn. We simultaneously collected electromyography recordings from bilateral implants in the pectoralis, supracoracoideus, biceps brachii and extensor metacarpi radialis muscles. The cockatoos maneuvered using flapping, banked turns with an average turn radius of 0.92 m. The mean rate of change in heading during a complete wingbeat varied through the turn and was significantly correlated to roll angle at mid-downstroke. Changes in roll angle were found to include both within-wingbeat and among-wingbeat components that bear no direct relationship to one another. Within-wingbeat changes in roll were dominated by the inertial effects while among-wingbeat changes in roll were likely the result of both inertial and aerodynamic effects.

Supplementary material available online at
http://jeb.biologists.org/cgi/content/full/210/11/1897/DC1

Key words: avian, maneuvering, biomechanics, flight, dynamics, *Eolophus roseicapillus*.

Introduction

Although the vast majority of the experimental work on the biomechanics of avian flight has focused on steady state flight, this focus owes much to the theoretical and experimental tractability of level, straight flight rather than its importance to the species under investigation (e.g. Brown, 1953; Tucker, 1973; Pennycuick et al., 1997; Tobalske et al., 2003). Many bird species spend much of their lives flying through dense, cluttered environments, and performance in these conditions may be as important to foraging (e.g. Evans and Thomas, 1992), survival and mating as minimizing the cost or maximizing the speed of straight line flight. While experimental studies of maneuvering flight are rare, the importance of maneuvering to fitness and as a measure of flight performance has been used to explain wing shape diversity in flying animals (Norberg and Rayner, 1987). For example, long thin wings have higher lift-to-drag ratios than shorter, thicker wings and are mostly found in seabirds that fly in open and uncluttered environments (Rayner, 1988). Other wing shapes may improve different facets of flight performance. For instance, shortening the wing and thereby reducing moment of inertia may improve maneuvering performance in flapping flight by increasing the flapping frequency (Norberg, 1981). Finally, several studies have shown that manipulation of the tail streamers of aerial insectivores such as the swallow (*Hirundo rustica*) can enhance or reduce performance in flight maze maneuvering experiments, likely *via* changes to the amount of lift and drag generated by the tail and therefore overall wing loading (e.g. Buchanan and Evans, 2000).

Existing theories relating wing and body shape to maneuvering performance are based on factors important to the performance of fixed wing aircraft such as wing loading and minimum gliding turn radius. While these factors no doubt influence maneuvering in flapping flight, their precise importance cannot be evaluated without a better understanding of the mechanisms used by flapping fliers to maneuver. Moreover, flapping fliers have many more degrees of freedom than fixed wing aircraft and may generate flight maneuvers with means outside the scope of fixed wing flight, such as right–left timing asymmetries in the wingbeat. Finally, birds

and other flying animals appear to lack the passive stability mechanisms common to fixed wing aircraft, such as a vertical rudder (Maynard Smith, 1952). This implies fine neuromuscular control of maneuvering flight, but few studies have attempted to identify the muscles involved in controlling maneuvers in vertebrate flight. In this study we use kinematic and electromyographic recordings of cockatoos executing a 90° turn at low speed to examine the aerodynamic mechanisms and underlying neuromuscular control of turning in birds, evaluating hypotheses based on the results of earlier studies.

Prior biomechanical studies of low speed turning in avian flight employed a variety of approaches, including three-dimensional (3D) kinematic analysis, electromyograms, and measurement of pectoralis force *via* a strain gauge mounted on the delto-pectoral crest of the humerus. These studies support somewhat different conclusions regarding the aerodynamic and neuromuscular mechanisms used by birds in maneuvering flight. A detailed 3D kinematic analysis of turning in pigeons (Warrick and Dial, 1998) found that the birds used banked turns with roll angle changing rapidly throughout the wingbeat cycle and roll accelerations and decelerations occurring within a single downstroke. Measured roll accelerations exceeded 1500 rad s^{-2} when averaged over a 20 ms time interval (~1/5th of a wingbeat). The kinematic pattern most strongly related to roll acceleration was right–left asymmetry in wrist velocity during downstroke and in the body coordinate system. Changes in wing shape or orientation were not associated with roll acceleration. These findings suggest that the pectoralis, the main downstroke depressor, is deeply involved in the generation of roll acceleration and therefore turning maneuvers. However, an electromyographic study of muscles in the wing and tail of turning pigeons (Dial and Gatesy, 1993) reported the greatest asymmetry in muscles surrounding the elbow and wrist; these apparently influenced wing pronation and flexion, conclusions counter to those reached by the detailed 3D kinematic study. Finally, a study of bilateral pectoralis force in turning pigeons (Warrick et al., 1998), reported small but persistent asymmetries in muscle force over the course of a turn. This finding confirms involvement of the pectoralis muscle in turning, but not the source of the asymmetry. Right–left asymmetry in pectoralis force might be the result of differences in pectoralis activation, differences in the aerodynamic forces that resist wing motion, or both.

Based on these prior studies, we made the following four hypotheses: (1) the cockatoos would turn by banking (rolling into the turn), (2) generating the necessary roll moments and therefore roll acceleration *via* wing velocity asymmetry early in downstroke. Additionally, we hypothesized that (3) these differences in wing velocity would be associated with asymmetries in the activation intensity, timing or duration between the right and left pectoralis muscles. As any one of these factors might be sufficient to generate a wing velocity asymmetry at different times in the stroke, we make no predictions as to the exact mode of asymmetry. Finally, we hypothesized (4) that higher resolution kinematics would allow detection of changes in wing shape and orientation complementary to the wing velocity asymmetries and indicated by earlier electromyographic results (Dial and Gatesy, 1993) but not found in the 3D kinematic study of pigeon turning (Warrick and Dial, 1998). As noted above, the pectoralis is the main wing depressor and the supracoracoideus the main wing elevator. The biceps brachii pronates the wing (Dial and Gatesy, 1993) while the extensor metacarpi radialis acts to extend the wrist and hand wing (Dial, 1992a). Both these actions could influence wing shape and orientation during the stroke, supplementing aerodynamic force asymmetries generated by the pectoralis.

Materials and methods

To address the hypotheses stated above, we collected high resolution, high-speed 3D kinematics from six rose-breasted cockatoos *Eolophus roseicapillus* Viellot making a slow, 90° turn through a maneuvering course. We simultaneously collected bilateral electromyograms (EMGs) from the pectoralis, supracoracoideus, biceps and extensor metacarpi radialis muscles.

Cockatoos

Five wild rose-breasted cockatoos were captured at the Waite campus of the University of Adelaide in Adelaide, South Australia. An additional cockatoo was purchased from a licensed animal dealer in Adelaide, resulting in a total of six birds (Table 1). The cockatoos were kept in individual pens (3 m×2 m×2.5 m, length×width×height) in an outdoor aviary at the University of Adelaide campus where they were provided with food and water *ad libitum*. The cockatoos were kept in captivity for a maximum of 2 weeks while the experiments were conducted. All training and experimental procedures were approved by the Harvard University Institutional Animal Care and Use Committee and the University of Adelaide Animal Ethics Committee.

Maneuvering course

The maneuvering course was a single 90° turn formed by the intersection of a 4 m×1 m×2 m (length×width×height) long flight corridor with a 3 m×1 m×2 m corridor (Fig. 1). The course was constructed of 4 cm diameter PVC pipe and fine plastic netting (2 cm square mesh). Perches constructed of PVC

Table 1. *Morphology*

	Mean ± s.d.	*N*
Total mass (g)	289.3±13.3	6
Proximal wing mass* (g)	21.2±0.8	4
Distal wing mass* (g)	6.2±0.4	4
Wing span (cm)	77.2±2.0	6
Wing area (cm^2)	861.4±20.5	6
Tail area (cm^2)	275.0±13.2	6
Pectoralis mass* (g)	29.9±1.3	4
Supracoracoideus mass* (g)	2.9±0.2	4

*For a single muscle or wing.

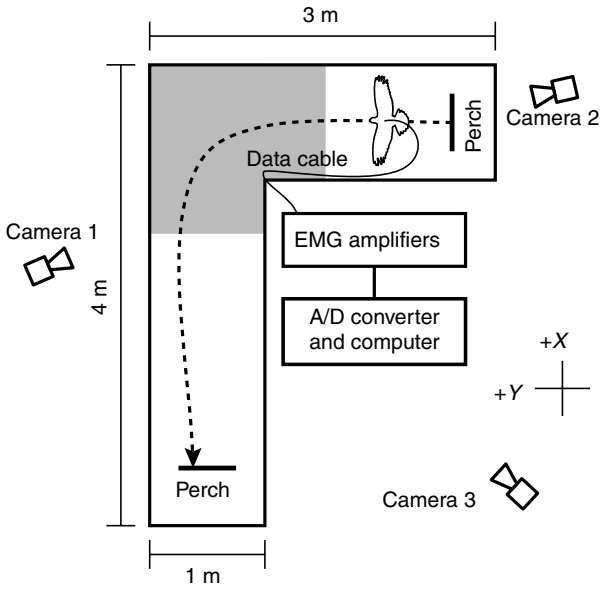

Fig. 1. An overhead view of the maneuvering course showing the position of the video cameras and recording devices. The cockatoo and course are to scale, the shaded region in the middle of the maneuvering course approximates the volume in view from which we were able to acquire 3D kinematics. X, Y, Earth fixed coordinates.

pipe were positioned at either end of the maneuvering course and the cockatoos were trained to fly through the course, navigating from perch to perch without contacting the maneuvering course netting walls. Cockatoos were trained to perform both left and right turns, flying through the course in both directions. The cockatoos readily learned to navigate the course; training typically required only a single 30 min session.

Electromyogram electrodes, implantation and digital recording

After anesthetizing the cockatoos to a surgical plane *via* isoflurane gas we implanted eight fine-wire bipolar hook electrodes (Loeb and Gans, 1986), placing them in the left and right pectoralis, supracoracoideus, biceps brachii and extensor metacarpi radialis muscles (Fig. 2). The electromyogram (EMG) electrodes were constructed of 0.004 gauge enamel-coated silver wire (California Fine Wire, Inc., Grover Beach, CA, USA), with 0.5 mm bared tips spaced 2 mm apart. After exposing the muscles *via* openings made in the skin overlying each location, the electrodes were implanted directly in the muscles using a 23-gauge hypodermic needle, and anchored to the muscle surface at the insertion site with 6-0 silk suture.

Following implantation, the electrode leads were passed under the skin to a common plug constructed of three 6-pin microconnectors bonded with epoxy and attached to the intervertebral ligaments in the center of the back. The back plug weighed 6.7 g. The EMG signals were transmitted to the amplifiers and recording equipment *via* a 3.6 m shielded cable, which the cockatoos pulled through the maneuvering course. During a typical trial, cockatoos supported 1.5 m (27.3 g) and accelerated up to 3 m (54.5 g) of cable. The mass of the back plug and accelerated cable were equal to 21% of the mass of the typical cockatoos. The EMG signals were amplified with Grass P511 EMG amplifiers (Astro-Med Inc., West Warwick, RI, USA) then recorded digitally at 10 kHz using a Kistler Bioware 3.0 system (Kistler Instrument Corp., Amherst, NY, USA). Following each experiment, the cockatoos were euthanized to permit verification of electrode placement. Good quality EMG signals were recorded from 35 of the 48 implants; most failures were due to the electrode wires breaking due to repeated bending near the shoulder joint.

Flight kinematics

Flight trials were recorded using three synchronized, high-speed digital video cameras (one Photron Fastcam-X 1280 PCI, Photron USA Inc., San Diego, CA, USA and two Redlake PCI 500, Redlake Inc., San Diego, CA, USA) operating at 250 frames s^{-1} with a shutter speed of 1/1000 s. The cameras were arranged around the maneuvering course such that the Photron camera recorded the wingbeats throughout the turn, while one Redlake camera recorded the bird early in the turn and the other recorded it finishing the turn (Fig. 1). The camera

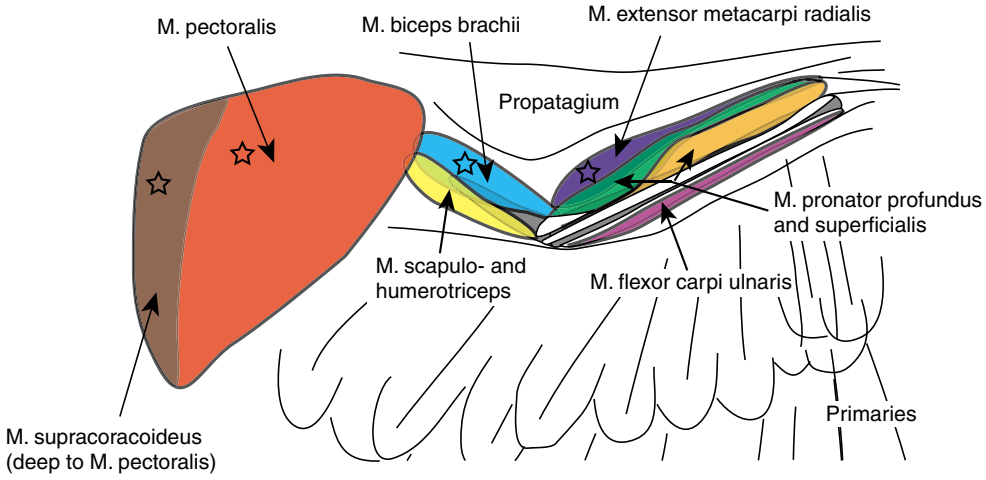

Fig. 2. We recorded electromyograms from the pectoralis, supracoracoideus, biceps brachii, and extensor metacarpi radialis muscles, shown here in ventral view along with the proximal portion of the wing. Stars mark implant locations.

data were synchronized to the EMG signals by recording the cameras' digital stop trigger together with the EMG amplifier outputs on the Kistler Bioware A/D system. The cameras were calibrated using the direct linear transformation (DLT) technique with a 56-point calibration frame (measuring 1.6 m×1.1 m×0.9 m in *xyz* coordinate space) that was recorded at the end of each set of trials (Hatze, 1988). In all cases, all trials for a particular bird were recorded in one session. The cockatoo was allowed to rest as necessary to maintain flight performance. Each cockatoo was marked with 1 cm diameter black spots with a white centre dot on the right and left tail (tip of the outermost retrices), wrist, and 9th primary tip. The spots were applied by lightly coating the area with white correction fluid and then coloring the correction fluid with black ink. In addition to these marked locations, the beak, EMG plug attachment and wing roots were digitized from the video images. All these locations were readily identified from the video images without resorting to markers.

Video records of four left and four right turns were digitized from each bird. In half of these trials (evenly divided among birds and directions), points were digitized for all video frames. In the other half of the trials the EMG plug attachment point was digitized in all frames, whereas the other points were digitized only in the seven frames surrounding mid-downstroke, defined as the frame with the greatest angle between the left and right wings. Digitizing and 3D reconstruction methodology generally followed that used in several prior studies of avian flight (e.g. Hedrick et al., 2004). In brief, the 3D reconstruction had a median root mean square error of reconstruction ranging from 0.40 mm at the beak to 1.48 mm for the right side 9th primary tip. Occasional gaps in the 3D point sequence were filled *via* spline interpolation, and all data were filtered with the 'Generalized Cross Validatory/Spline' (GCVSPL) program (Woltring, 1986). The spline smoothing coefficients were adjusted to produce a filter cut-off frequency of approximately 37 Hz, nearly five times greater than wingbeat frequency. First and second order derivatives of positional data were computed from the spline coefficients. The partially digitized trials were treated similarly, except that analysis was restricted to the seven frames surrounding mid-downstroke, during which all points were always in view and no interpolation of missing data was required.

Frames of reference and coordinate systems

Two frames of reference and two coordinate systems were used in the analysis of the kinematic data. The first of these was the world reference frame, an Earth fixed coordinate system *XYZ* with *X* and *Y* along different axes of the flight course (Fig. 1) and +*Z* pointing up. These were transformed *via* a set of Cardan angles (pitch, roll and yaw) to a standard, anatomical (or body) coordinate system $X_bY_bZ_b$ with $+X_b$ extending anterior, ahead of the bird, $+Y_b$ lateral along the left wing, and $+Z_b$ upward (Fig. 3A). This coordinate system was centered on the midpoint of the left and right wing roots. The Y_b axis passed through the two wing roots and the EMG plug attachment lay in the X_b–Y_b plane. We also transformed the Cartesian $X_bY_bZ_b$ coordinates of the wing points to a spherical coordinate system of wing sweep angle θ (Fig. 3B), wing elevation angle ϕ (Fig. 3C), and radius *R*.

Additional kinematic parameters

In addition to the velocities and orientations described earlier, we also calculated the instantaneous heading and the rate of change (first derivative) of heading. Heading, the direction of the cockatoo's motion in the *X*–*Y* plane of the world coordinate system, was computed from the instantaneous velocity of the plug attachment point. Heading derivatives were calculated using the GCVSPL program described earlier, but with an assumption of no error and therefore no additional filtering.

In some cases, power spectra were computed for different kinematics through time and within an individual trial. Power spectra were computed from kinematic time series with the linear trend removed. Finally, 4-pole zero-lag digital Butterworth bandpass filters were applied to portions of the kinematic data to reveal the amplitude of motion within particular frequency ranges. In these cases we note the passband range when describing the data.

We created a kinematic data set containing only the among-wingbeat changes in roll angle by fitting a quintic spline to the body roll angles recorded at mid-downstroke. Among-wingbeat roll angle derivatives were computed from the spline fit. In addition to removing the high-frequency inertial component of instantaneous roll, this approach greatly reduces the number of digitized video frames required to analyze a trial because the partially digitized trials (described earlier) contain all the information required for a mid-downstroke to mid-downstroke interpolation.

Electromyogram analysis

All numeric analysis of the EMG signals was carried out in MATLAB 7.0 for Linux (Mathworks Inc., Natick, MA, USA).

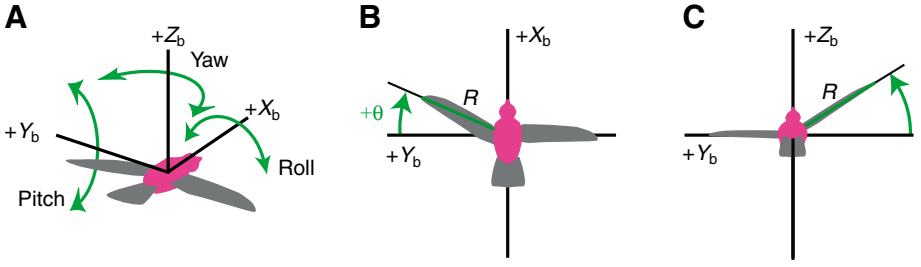

Fig. 3. (A) The local or anatomic coordinate system $X_bY_bZ_b$ along with the roll, pitch and yaw axes. (B) Wing sweep angle (θ). Note that θ is positive for forward sweep of both the right and left wings. (C) Wing elevation angle (ϕ), which is positive for elevation of both the right and left wings. *R*, radius.

Prior to analysis, the raw EMG signals were bandpass filtered from 30 to 1600 Hz using a digital Butterworth filter to remove noise from the bird's movements and from the computers used to acquire the EMG and video data. Power spectrum analysis of the EMG bursts indicated that a majority of the signal power fell between 500 and 1000 Hz; the precise distribution varied somewhat between different implants. The EMG bursts were then characterized by the following attributes: (1) activation duration, (2) activation and deactivation time relative to the activation time of the right pectoralis muscle, (3) mean spike amplitude (MSA), (4) the rectified burst impulse (the MSA multiplied by burst duration), and (5) the fraction of the burst required to reach one half of the rectified burst impulse. Because differences in electrode geometry and recording site among individual EMG electrodes lead to differences in the voltage magnitude recorded from a given implant (Loeb and Gans, 1986), we normalized the MSA data prior to further analysis by subtracting the mean MSA for that implant across all trials and then dividing by the standard deviation. This compensated for differences in offset or gain between birds. The same approach was used to normalize the rectified burst impulse from each muscle.

Wingbeat numbering and consolidation

The number of wingbeats required to complete the course varied among trials and individuals. To facilitate comparison between trials and within individuals, the wingbeats were re-numbered such that the wingbeat with the mid-downstroke heading closest to a 45° change from the initial heading became number 0. The other wingbeats were numbered sequentially from this basis. On occasions where a single value characteristic of the kinematic measurements for an entire wingbeat was required, i.e. velocity during the first wingbeat, we used the average value for the entire wingbeat, unless otherwise noted.

Following re-numbering based on the mid-turn wingbeat, we consolidated the kinematic data by creating a mean right turn and mean left turn for each bird from the mean values at a given wingbeat number in each direction. This left a data set of approximately 60 consolidated wingbeats for further analysis. In most cases the kinematic measurements of interest were the differences between the right and left (or outside and inside) wings. Because all kinematic measurements were available for both wings from all wingbeats, this requirement did not pose a problem for the kinematic analysis. This was not the case for the EMG analysis, because in several cases data were acquired from one but not both muscles of a bilateral pair, and therefore right–left differences were not available. To overcome these difficulties, we employed a slightly different consolidation routine for the EMG data.

We consolidated the EMG data to a set of mean outside wing (or muscle) and inside wing differences. First, the EMG and kinematic measurements for each individual muscle and the single wing kinematic parameters were consolidated to an average set for a given turn direction, as described above for the kinematic data. Following this, the data were further consolidated by subtracting the measurements from the inside of a turn from those taken for the same muscle when on the outside of the turn. These operations allowed us to make useful comparisons in situations where good recordings were available from only one muscle of a pair. Additionally, the EMG consolidation routine resulted in comparisons between the same muscle in different conditions (i.e. outside wing of the turn *versus* inside wing of the turn), rather than different muscles in the same circumstance. This eliminates many of the problems associated with inter-EMG differences due to the precise implant location and geometry. These operations reduce the number of wingbeats available for EMG analysis to a maximum of approximately 30, or fewer for cases with missing data from both right and left muscles.

Statistics

Statistical analysis in this paper was limited to linear regression and partial linear regression analyses relating different measures of kinematic or electromyographic asymmetry to changes in body orientation or flight direction. All computations were performed in MATLAB 7.0. The consolidated wingbeats from each individual represent a time-series of flaps, raising the possibility that successive wingbeats in the turn sequence were not independent. In general, this was the case for measurements of position and orientation, but not for their derivatives or any of the kinematic or EMG asymmetries. Correlations between successive measures of position were always greatest at a lag of one wingbeat. To avoid overestimating the strength or significance of the relationship between variables, in cases where one of the variables of interest was temporally non-independent we included it at a +1 wingbeat lag as an additional predictor in a partial regression analysis.

Inertial reorientation within and among wingbeats

While flapping their wings through different arcs, flying organisms experience transient changes in angular orientation. For constant moments of wing inertia, these transient changes cannot generate a net change in orientation. However, because the wings of birds and bats flex at the wrist joint during upstroke and therefore have time-varying moments of inertia, they can generate net changes in orientation without any change in net angular momentum. This process is similar to the one used by a cat to right itself while falling (Frohlich, 1980). Appendix 1 develops a set of equations for computing the magnitude of inertial reorientation, assuming that the wing moments of inertia vary only once per cycle, at the transition between downstroke and upstroke.

Rigid body simulations

In addition to the simplified treatment of inertial reorientation described in Appendix 1, we also used a simple simulation of a flying bird to explore the inertial consequences of asymmetric flapping. The simulation was written in the Python programming language using the pyODE interface to the Open Dynamics Engine, a freely available physics

Table 2. *Moments of inertia*

	I_x	I_y	I_z
Body only (cm^2 g)	1685.5	4447.3	4447.3
Body with wings fully extended (cm^2 g)	12888.9	4545.3	12953.4
Body with wings flexed (cm^2 g)	8654.1	5466.8	1278.6
Extended wing about the shoulder (cm^2 g)	3417.6	–	–
Flexed wing about the shoulder (cm^2 g)	1880.0	–	–
Body with one extended wing about the opposite shoulder (cm^2 g)	11786.6	–	–
Body with one flexed wing about the opposite shoulder (cm^2 g)	9000.1	–	–

Table 3. *Wing profile*

Section	Distance from shoulder (cm)	Area (cm^2)	Mass (g)
1	1.5	27.41	5.77
2	4.5	35.18	4.44
3	7.5	32.34	4.89
4	10.5	34.98	3.16
5*	13.5	36.19	2.91
6	16.5	37.68	1.63
7	19.5	36.12	1.73
8	22.5	35.51	1.10
9	25.5	33.54	0.61
10	28.5	31.68	0.44
11	31.5	28.86	0.32
12	34.5	23.06	0.24
13	37.5	16.51	0.08

*The 5th section is the last in the proximal wing.

simulation environment. Source code for the simulation is available upon request. The simulated bird was constructed from a body, four wing sections and four hinge joints. Each of the body and wing segments had a realistic mass and moment of inertia tensor derived from measurements of the cockatoos (Table 2, Table 3). The left and right wings were each composed of a proximal and distal segment connected by a passive hinge joint with limited range of motion appropriate for the wrist. The proximal wing sections were each attached to the body *via* an actuated hinge joint, the shoulder. We simulated flapping by specifying the instantaneous angular velocity of the proximal wing segments about the shoulder. Wingbeat frequency (7.5 Hz), left wing amplitude (90° peak to peak), and right wing amplitude (70°) were based on values taken from the kinematic recordings (see below). We simulated a null gravity environment and did not include any aerodynamic forces; therefore, all instantaneous and net changes in body orientation were solely the result of inertia.

Results

Whole turn performance

The cockatoos navigated the maneuvering course in a broadly stereotyped manner with the number of wingbeats required to complete the course ranging from 10 to 15 among individuals. Turn radius was constrained by the course layout and averaged 0.92±0.09 m (inter-individual mean ± s.d., N=6). Mean flight speed through the turn was 3.01±0.21 m s^{-1} and tended to decline through the turn. Speed in wingbeat number –3, the first typically recorded by the cameras, averaged 3.46±0.56 m s^{-1} but declined to an average of 2.72±0.59 m s^{-1} by the completion of the turn (wingbeat number +3). Average rate of change in heading through the entire turn was 154.1±13.54 deg. s^{-1}. Mean wingbeat frequency was 7.7± 0.58 Hz, with downstrokes being longer in duration than upstrokes (by a factor of 1.48±0.09). The cockatoos tended to maintain potential energy through the turn, as we found no regular changes in altitude before, during, or after the turns.

Average rate of change in heading during a complete wingbeat varied through the turn from a minimum near zero in wingbeat number –3 to a peak of approximately 320 deg. s^{-1} during the wingbeat closest to the midpoint of the turn, the 0th wingbeat. These changes in heading correspond to whole-wingbeat centripetal accelerations ranging from near zero for the –3rd wingbeat to 10.4 m s^{-2} in the 0th wingbeat.

Patterns of change in orientation

Changes in orientation occurred throughout the turn, with each half-stroke typically encompassing both increases and decreases in roll, pitch and yaw (Fig. 4). The birds consistently rolled into the turn over the course of several wingbeats, typically reaching a maximum roll angle of greater than 40° by the mid-turn wingbeat before beginning to roll back to the level. Changes in yaw also occurred systematically during the turn, with the net change in yaw encompassing the 90° change in direction required by the turn. Changes in roll and yaw did not have any consistent temporal relationship; on some occasions changes in roll appeared to precede changes in yaw, while in other wingbeats the opposite occurred. While changes in yaw were clearly required to keep the bird's body axis oriented parallel with its heading (direction of travel), at the more extreme roll angles adopted at mid-turn, changes in pitch were also required. These were manifest as a greater than typical pitch in the wingbeats with the greatest body roll (i.e. Fig. 4, wingbeat 1). Aside from this, and a tendency in three of the six birds to pitch up by 8–19° in the wingbeat just prior to the turn, there were no consistent changes in pitch across the entire turn.

Wingbeat asymmetries in turning

We found numerous asymmetries in the wing kinematics of the turning cockatoos (Fig. 5). The majority of these asymmetries were in the amplitude of the wing stroke rather than the timing, with right–left differences in peak to peak amplitude exceeding 20° at the wrist and 30° at the tip on

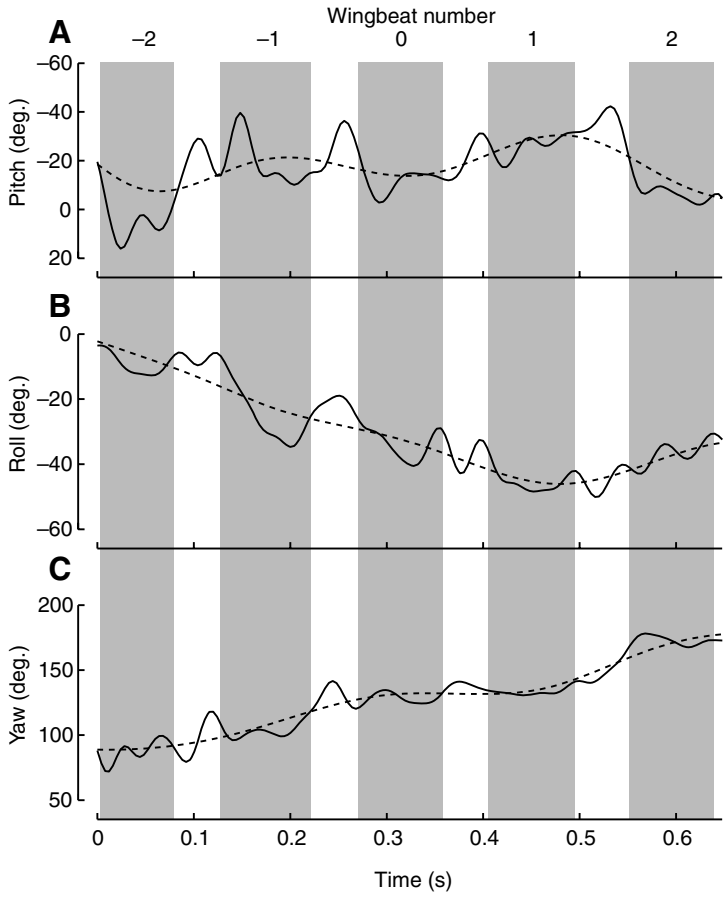

Fig. 4. (A) Body pitch, (B) roll and (C) yaw orientation through five wingbeats of a turn. Wingbeats are numbered across the top of the figure, with wingbeat 0 falling at mid-turn. Downstrokes are shaded gray. Solid lines are the data subject to normal processing, i.e. a 37 Hz low-pass filter. Broken lines were processed with a 4 Hz low-pass filter to show only the inter-wingbeat changes in orientation. Note negative pitch is 'beak up' in the body coordinate system we used, thus the inverted axis in A.

occasion. The arc swept by the tip in both wing elevation (ϕ) and sweep angles (θ) was typically greater than that of the wrist, largely because at the end of downstroke the wrist begins moving back above and behind the body while the wrist joint flexes, allowing the tip to continue traveling below and ahead of the body. Asymmetries in wing position were most apparent at the beginning and end of the half-strokes and least prominent at mid-upstroke and mid-downstroke (Fig. 5). However, the asymmetries in stroke amplitude lead to asymmetries in stroke velocity, which were greatest at mid-downstroke when overall wing velocity magnitudes were greatest.

Timing of changes in heading

Changes in heading largely occurred during downstroke, with the peak rate of change typically falling at mid-downstroke (Fig. 6). Peak instantaneous rates of change in heading were slightly greater than 400 deg. s^{-1} and typically occurred at mid-downstroke in the 0th or 1st wingbeat of the turn. The average rate of change in heading of the 0th wingbeat during downstroke was 270.1±26.5 and 113.4±30.5 deg. s^{-1} during upstroke (inter-individual mean ± s.d., N=6). For all recorded wingbeats, the rate of change in heading during downstroke was 2.08±0.38 times greater than in upstroke, with no regular change in this proportion during the turn. The instantaneous rate of change in heading also typically reached a local minimum near the mid-point of the upstroke. Due to the predominance of changes in heading during downstroke *versus* that in upstroke, much of the subsequent analysis examines associations between changes in heading during downstroke and specific kinematic or EMG measurements.

Kinematic predictors of the rate of change in heading

We found that the mean rate of change in heading during downstroke was well predicted by the roll angle at mid-downstroke (Fig. 7, r^2=0.95, P<0.00001). Yaw rate at mid-downstroke was significantly correlated with the average rate of change in heading during downstroke (r^2=0.70, P<0.001) (i.e. the cockatoos yawed into the turn), but was also strongly correlated with roll angle (r^2=0.62, P<0.01). The partial correlation between roll angle and rate of change in heading with yaw rate included as an additional predictor was significant (r^2=0.79, P<0.001, two-tailed t-test). However, its complement, the partial correlation of yaw rate to rate of change in heading with roll angle included as an additional predictor, was not significant (r^2=0.21, P>0.05, two-tailed t-test).

Changes in roll within and among wingbeats

Initial examination of the instantaneous body roll angle during the turns showed that roll angle changed throughout each turn and included both within- and among-wingbeat components (Fig. 8A). A power spectrum analysis (Fig. 8B) showed that variation in roll angle occurred predominantly at frequencies less than one-half wingbeat frequency and at wingbeat frequency. We separated the portion of variation occurring at wingbeat frequency from the rest of the signal using a bandpass filter (4-pole digital Butterworth, zero lag, cut-offs of 4 and 10 Hz; Fig. 8C), finding a maximum peak-to-peak amplitude of approximately 16°. The large amplitude of the wingbeat frequency component was characteristic of all trials. Furthermore, while the mean roll velocity for a whole stroke was small, and the instantaneous roll velocities and accelerations were large, reflecting the large amplitude of the wingbeat frequency component of changes in roll through time. For example, the mean absolute value of the rate of change in roll angle from mid-downstroke to mid-downstroke, i.e. the whole stroke roll velocity, was 117.3±27.0 deg. s^{-1} (N=60), but the corresponding measurement from the start of downstroke to the middle of downstroke was 236.4±72.8 deg. s^{-1} (N=60); the other quarter-stroke intervals had similarly high mean roll velocities.

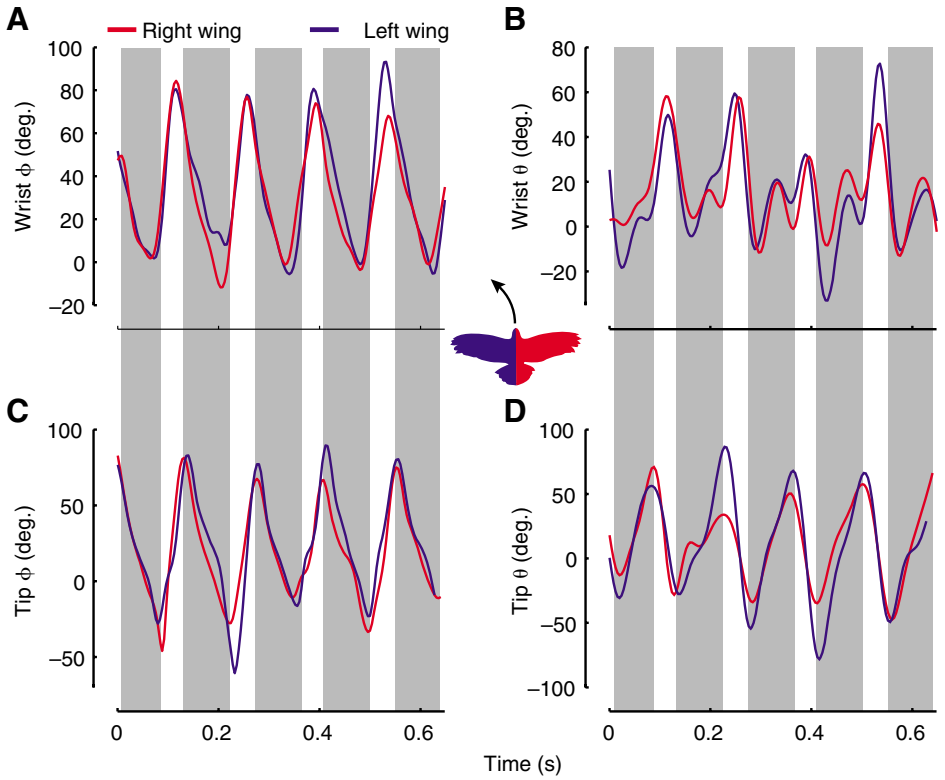

Fig. 5. Wing angles (see Fig. 3) through five wingbeats of a left turn. (A) Wing elevation angle (ϕ) and (B) sweep angle (θ) measured at the wrist. (C) Elevation and (D) sweep angle measured at the tip. Both the wrist and tip angles contained right–left asymmetries throughout the wingbeat sequence. Asymmetries in position were most prominent at the stroke transitions and were much reduced by mid-stroke. Measurements made at the wrist typically encompassed a smaller range than measurements made at the tip because wrist flexion allows the tip continues to move ahead and below the bird near the end of downstroke while the wrist slows or even reverses direction.

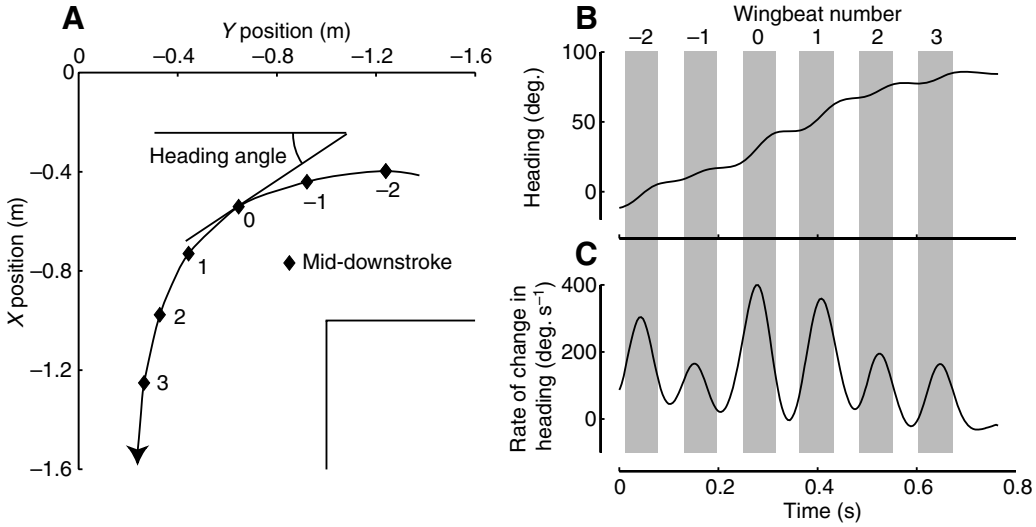

Fig. 6. (A) An overhead view of an example flight through the maneuvering course (see Fig. 1) with numbered wingbeats, showing instantaneous heading at wingbeat 0. The numbered wingbeats correspond to the numbers between sections B and C. (B) Change in heading through time; gray shading indicates downstroke. (C) Rate of change in heading, the derivative of section B with respect to time. Changes in heading occur predominantly during downstroke.

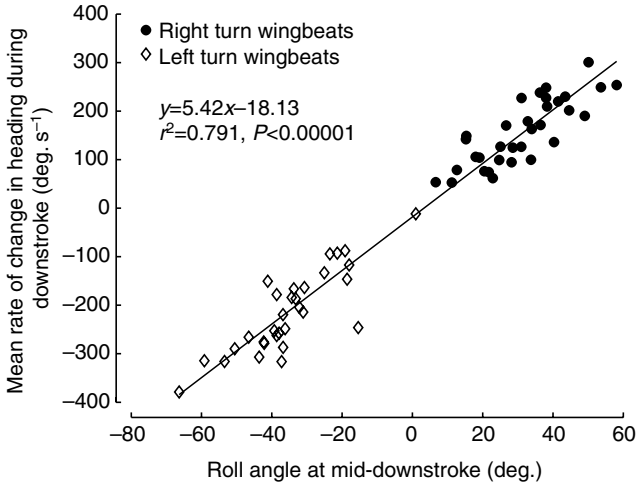

Fig. 7. The mean rate of change in heading during a stroke was closely related to the roll angle measured at mid-downstroke. Individual points are the average response of a bird for a given wingbeat number and turn direction; N=59. Although the regression line and equation represent a simple linear regression between the two measurements, the r^2 and P values reflect the partial correlation between the two variables, controlling for the temporal non-independence of roll angle as described in Materials and methods. The r^2 for the simple linear regression was 0.953 with P<0.00001 and F=1264.

Moreover, the magnitudes of roll velocity (and acceleration) during different partial stroke intervals were not significantly correlated with whole stroke roll velocity (P>0.05, two-tailed t-test).

Inertial reorientation within- and among- wingbeats

Applying Eqn A3 and Eqn A5 from Appendix 1 to the moment of inertia data from Table 2 and wingbeat arcs of 90° and 70°, typical values for the most asymmetric wingbeats that were employed in trials recorded in this study, resulted in a maximum transient change in orientation of 5.8° and a net change of 1.6° for a complete wingbeat cycle. These estimates, based on a single change in wing moment of inertia per wingbeat cycle, simplify the case of a flapping bird where moments of inertia change continually throughout the wingbeat. To examine how these instantaneous changes might

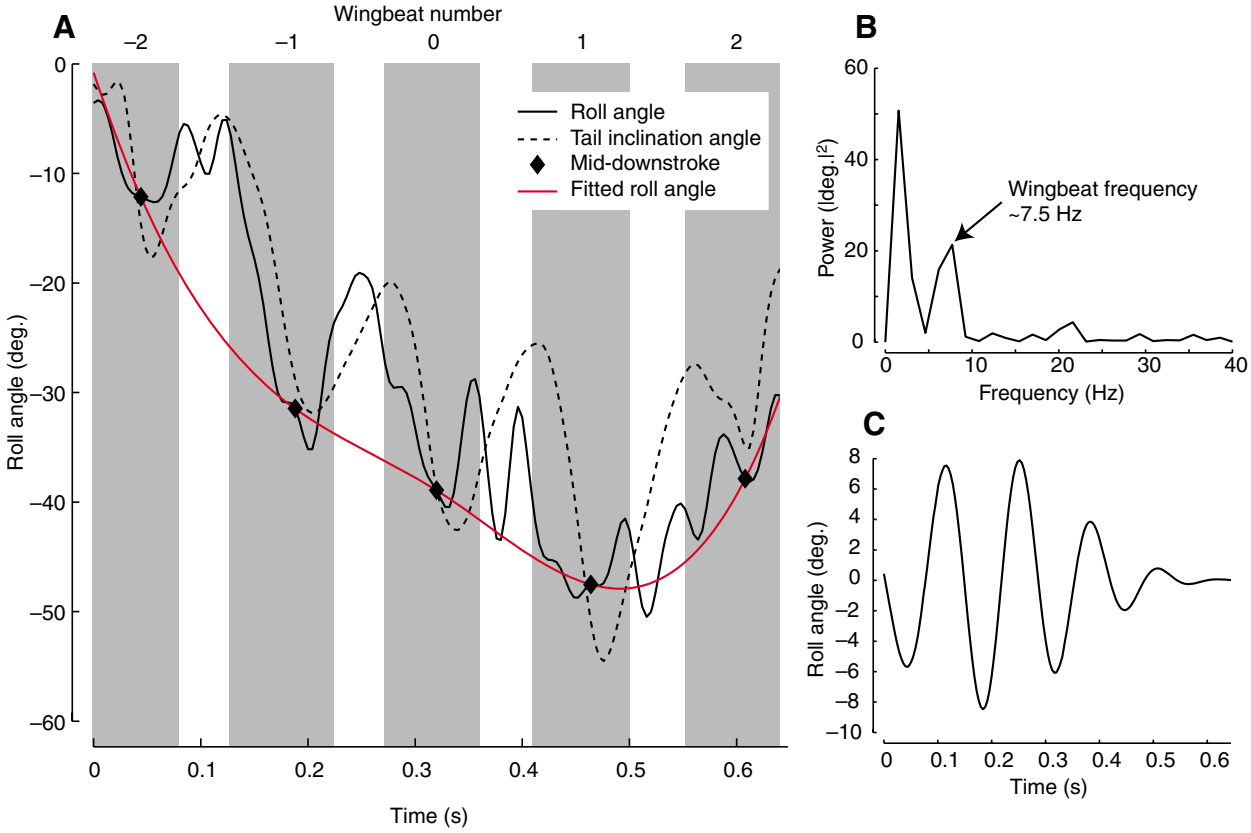

Fig. 8. Roll orientation through a left turn. (A) Changes in roll angle through time during a single trial, measured at the wing roots (Roll angle) and at the tail (Tail inclination angle). Roll angle changes both within and among wingbeats, typically reading a local minimum at mid-downstroke as the wings pass through the horizontal plane of the body coordinate system. (B) The power spectrum of the roll angle reveals that changes are largely confined to two frequencies, the bird's wingbeat frequency and a lower frequency encompassing approximately 3 wingbeats. (C) The peak-to-peak amplitude of the changes in roll near wingbeat frequency were approximately 16° and declined as the bird neared the end of the turn. In contrast, the peak-to-peak amplitude of the lower frequency, approximated by the red line in A, was approximately 45°.

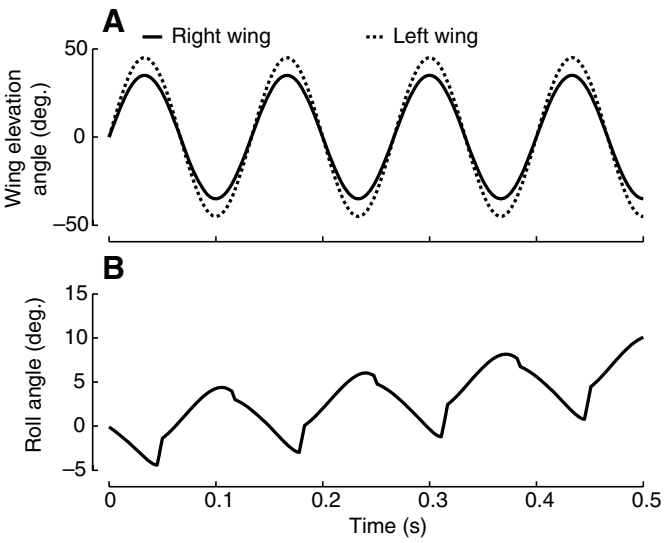

Fig. 9. The simple physics simulation of a flapping cockatoo shows that asymmetric flapping causes instantaneous changes in roll angle. (A) The wing elevation angles used in the simulation. The amplitude difference of 20° approximates the larger amplitude asymmetries used by the turning cockatoos. (B) The roll angle associated with the asymmetric wing elevation angles. The simulated cockatoo has body and wing masses and moments of inertia identical to those collected from the cockatoos in the study, but flies in a null-gravity environment and generates no aerodynamic forces. Thus, all changes in roll orientation are due to the torque required to flap the wings. The somewhat non-sinusoidal behavior in the roll angle result is due to the passive hinge joint at the wrist. An animation of this simulation is available in supplementary material.

affect the degree of inertia reorientation, we constructed a linked rigid-body simulation of a flapping bird (see Materials and methods). As shown in Fig. 9, simulated flapping with an amplitude asymmetry generated changes in the body roll angle of approximately 8.8° peak-to-peak amplitude and 2.0° among-wingbeat change.

Kinematic correlates to within- and among-wingbeat roll acceleration

Our separate measures of within- and among-wingbeat roll acceleration were not correlated with one another, but were each related to different kinematic asymmetries. Within-wingbeat roll acceleration, measured as the instantaneous roll acceleration at one quarter downstroke in the fully digitized trials, was significantly correlated with the right–left difference in wrist velocity in the body coordinate system, also measured at one quarter downstroke (r^2=0.40, P<0.00001; Fig. 10A). The correlation was such that greater right-side wrist velocity was associated with instantaneous roll acceleration to the left. Correlations were evaluated at one quarter downstroke, i.e. at the midpoint of the first half of downstroke, because angular accelerations due to wing inertia should approximate zero at mid-downstroke.

Among-wingbeat roll acceleration was significantly correlated with the right–left difference in wrist velocity in the world coordinate system (r^2=0.34, P<0.00001; Fig. 10B) but not to wrist velocity in the body coordinate system. A number of other kinematic measurements based on visually apparent asymmetries were not significantly related to roll acceleration in either the world or body coordinate systems (Fig. 11). These

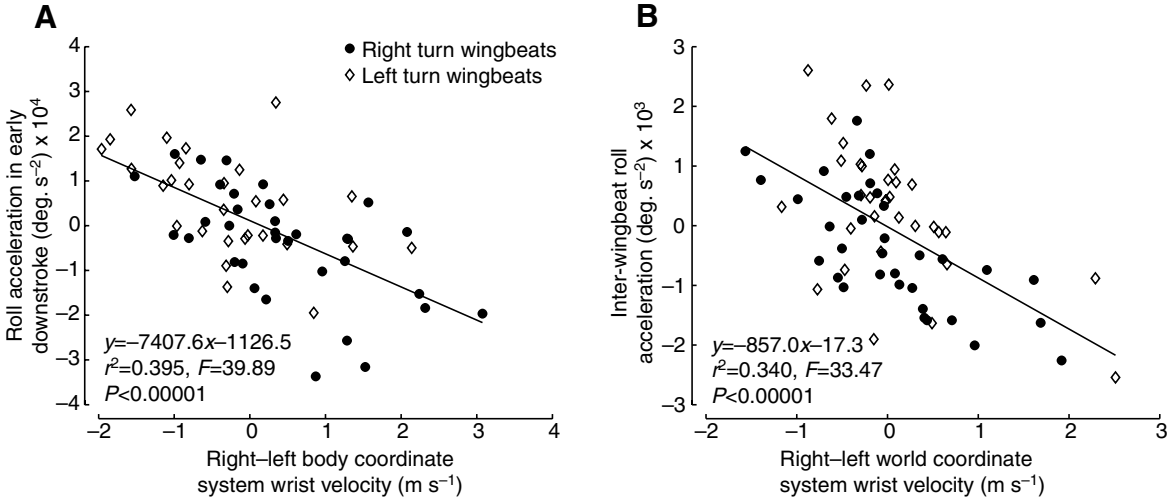

Fig. 10. (A) Relationship between instantaneous roll acceleration, measured at the midpoint of the first half of downstroke, and the difference in wrist velocity in the body coordinate system, measured at the same time. (B) Relationship between inter-wingbeat roll acceleration and the difference in world coordinate system wrist velocity at mid-downstroke. Note that the *y*-axis scale in A is an order of magnitude larger than that in B. In general, within-wingbeat roll accelerations were due to inertial effects and therefore related to movements in the body coordinate system. Inter-wingbeat roll accelerations include an aerodynamic component and therefore should be related to velocities in the world coordinate system. The instantaneous and inter-wingbeat roll accelerations were not correlated with one another, nor were the wrist velocity differences measured in the two coordinate systems.

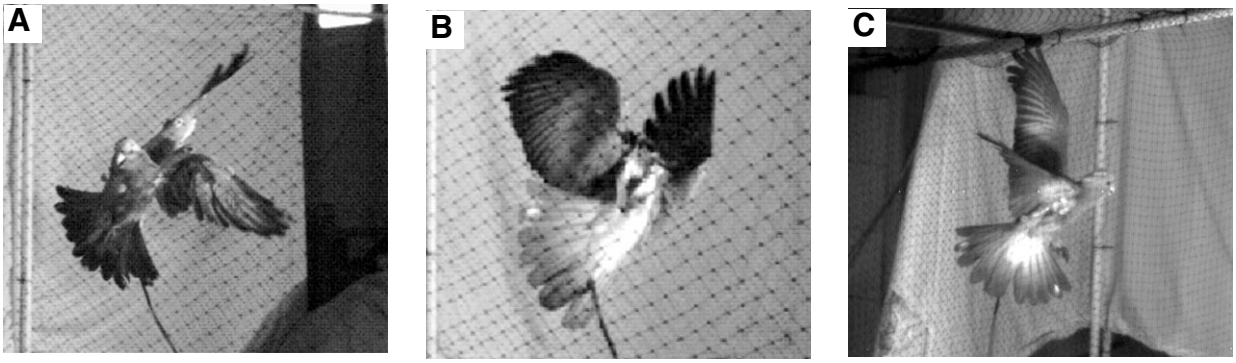

Fig. 11. We observed a number of asymmetries in the wing kinematics of the cockatoos as they navigated the maneuvering course, including but not limited to the following. (A) Asymmetric wrist flexion angles at the start of downstroke, (B) asymmetric wrist angles and wingtip trajectories at the end of downstroke, and (C) asymmetric wing velocity vectors angles at the start of downstroke. These asymmetries all occur in the 3D reconstruction as well as the 2D projections given by the camera, although the camera views do accentuate some asymmetries. However, none of these asymmetries was significantly correlated with changes in heading or roll.

include the right–left difference in wrist flexion angle at the start of downstroke, the difference in wing velocity vectors in the body coordinate system, and the difference in wrist flexion angles at the end of downstroke.

Overall muscle activation patterns

As has been described in prior studies (Dial, 1992a; Dial, 1992b), we found that the pectoralis, biceps brachii and extensor metacarpi radialis were activated during downstroke and the supracoracoideus during upstroke (Fig. 12). Activation of the three downstroke muscles began at mid-upstroke and preceded the kinematic beginning of downstroke by approximately 0.025 s (approximately 1/5th of a wingbeat cycle). This delay between muscle activation and the kinematic

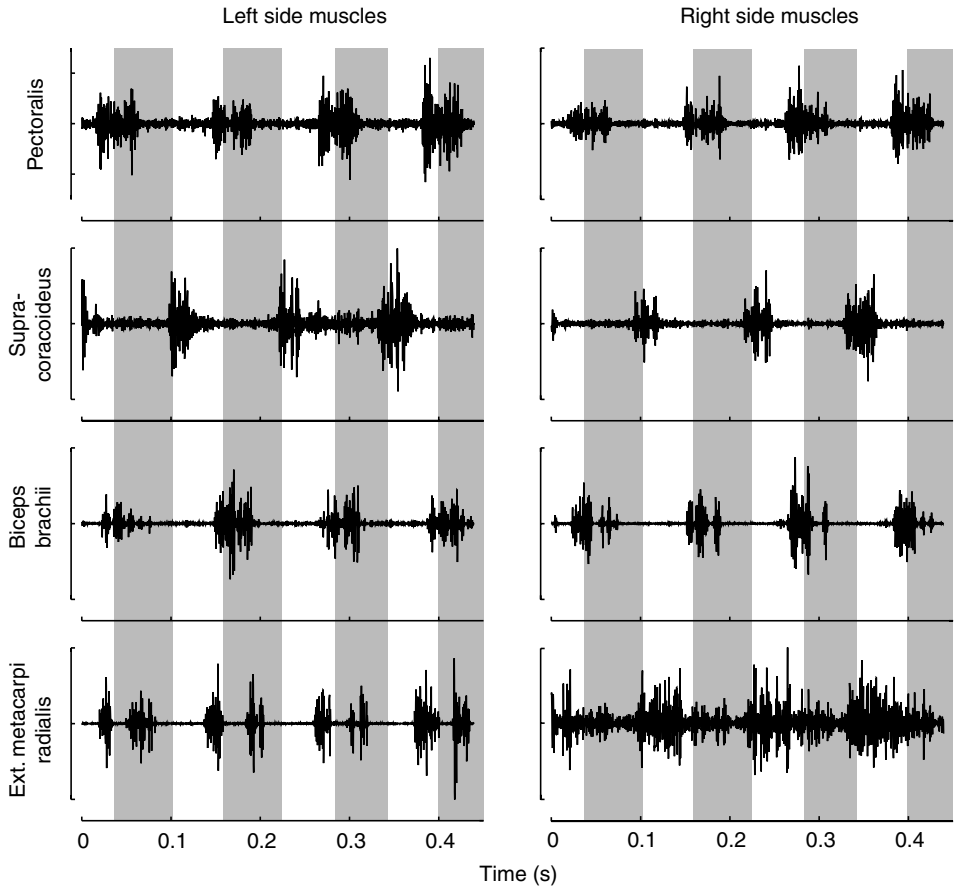

Fig. 12. Sample EMG sequence with shaded bars indicating the kinematic downstroke. The pectoralis, biceps and extensor metacarpi radialis were all generally activated approximately 0.025 s prior to the kinematic downstroke; activation in these three muscles ceases at approximately mid-downstroke. The supracoracoideus was typically activated just prior to the end of the kinematic downstroke and ceased activation near the middle of the kinematic upstroke just prior to the beginning of downstroke activation. Note that the right extensor metacarpi radialis recording in this example was from a failed implant.

stroke cycle is also characteristic of avian flight and likely represents both the time required for the muscles to begin shortening when activated while lengthening and the temporal delay between downward movement of the humerus relative to motion of the wrist and hand wing. The supracoracoideus was activated shortly before the beginning of upstroke; activation ceased near the kinematic mid-upstroke with the humerus fully elevated but the wrist joint flexed at an approximately 90° angle. The end of supracoracoideus activation coincided almost exactly with the beginning of pectoralis activation.

We found that the largest muscles measured, the pectoralis and supracoracoideus, exhibited the smallest degree of asymmetry, both between left and right muscles and from wingbeat to wingbeat. The pectoralis activation patterns were especially consistent; the coefficient of variance of the burst duration was 0.11, i.e. the standard deviation of the duration was approximately 1/10th of the mean duration. Similarly, the coefficient of variation for the pectoralis mean spike amplitude was 0.23. In contrast, smaller muscles such as the biceps were more variable; the coefficient of variation for biceps burst duration was 0.17 and for mean spike amplitude was 0.31. These differences likely reflect both the ease of making repeated high quality EMG recordings from a particular muscle and the degree to which a muscle is subject to functional constraint.

Muscle activation versus changes in heading and body orientation

We found no significant correlations between any muscle activation parameters and the among-wingbeat changes in heading or body orientation. However, a number of pectoralis measures, most prominently the outside – inside difference in impulse (quantified as the rectified and integrated EMG burst), were significantly associated with the within-wingbeat roll acceleration (r^2=0.23, P<0.05), such that a larger EMG burst impulse from the outside pectoralis was correlated with roll acceleration to the inside. Other associated pectoralis activation measures were not significant once the EMG impulse difference was included as a partial correlate. The difference in pectoralis burst area was also a good predictor of the difference in wrist velocity in the body coordinate system (r^2=0.30, P<0.01), with a greater pectoralis burst area correlated with a greater wing velocity. Despite these relationships, no pectoralis activation measurements were associated with wrist velocity differences in the world coordinate system or with among-wingbeat roll acceleration.

Discussion

We found that the cockatoos executed 90°, low-speed turns by banking (rolling) into the turn, thus redirecting a portion of the net aerodynamic force generated by the wings and leading to a change in heading. The cockatoos experienced wide variation in roll within a single wingbeat, as well as changes in roll across several wingbeats. Because the cockatoos continued rolling in the same direction for several wingbeats, both the within- and among-wingbeat changes in roll orientation were important to completion of the turn. This finding confirmed the first of our hypotheses, the use of roll-based turns similar to those described in previous studies of low speed avian maneuverability.

Kinematic predictors of roll acceleration

In partial support of our second initial hypothesis and the results of Warrick and Dial (Warrick and Dial, 1998), asymmetry between the right- and left-wrist velocities in the body coordinate system was a significant predictor of within-wingbeat roll acceleration. Additionally, asymmetry in wrist velocities in the world coordinate system was predictive of among-wingbeat roll acceleration. However, within-wingbeat roll acceleration was not correlated with among-wingbeat roll acceleration, and right–left asymmetries in wrist velocity in the body coordinate system were not correlated with the equivalent measurement in the world coordinate system. Note that only the asymmetries in wrist velocity between the two coordinate systems were not correlated. The velocity of an individual wrist in the body coordinate system was strongly correlated with the velocity of the same point in the global coordinate system, but right–left differences in velocity were not correlated.

The two measurements of wrist velocity asymmetry separately predict the within-wingbeat and inter-wingbeat roll accelerations, suggesting that roll accelerations at these different timescales were the result of distinct mechanisms. Changes in roll due to inertial effects, a possible source of the within-wingbeat roll acceleration (see below), should be related to wing velocities and accelerations in the body coordinate system, as was found in this study and in that of Warrick and Dial (Warrick and Dial, 1998). In comparison, changes in roll due to aerodynamic effects should depend in part on velocity asymmetries in the world coordinate system, as these velocities influence the air flow velocity over the wing and thus the magnitude of aerodynamic forces acting on the wing. Therefore, the relationship between world coordinate system wrist velocity asymmetry and inter-wingbeat roll acceleration was not surprising.

The kinematic predictors of roll acceleration, both within- and among-wingbeat, were weak, with r^2 values of 0.40 and 0.34, respectively. However, neither measurement contains all the information necessary to estimate torque from either inertial or aerodynamic sources. For example, aerodynamic torque asymmetries might be due to differences in wing shape, orientation and position as well wing velocity in the body coordinate system. None of these measures, apart from wrist velocity, were found to be significant predictors of acceleration when considered in isolation, thus rejecting our fourth initial hypothesis, but might provide additional predictive power when combined with one another. We develop an integrated model of turning flight, which combines several kinematic measures into an estimate of aerodynamic torque, and evaluate it in comparison to the cockatoo data, in the companion paper (Hedrick et al., 2007).

Neuromuscular control of turning

We did not uncover any link between the different muscle activation parameters studied and the among-wingbeat changes in roll crucial to turning flight, or to overall changes in heading, and thus did not fully support any of our initial hypotheses on the importance of muscle activation asymmetries. This is not to say that asymmetries were not present, only that we found no asymmetries that were significantly correlated to overall maneuvering performance. On the contrary, none of the muscles examined here were perfectly symmetric and, as described above, asymmetries in the pectoralis impulse were significantly correlated to both within-wingbeat roll acceleration and asymmetries in wrist velocity in the body coordinate system. However, neither of these parameters was significantly associated with among-wingbeat roll acceleration, an important part of the overall turning maneuver.

The absence of correlation between individual, per-wingbeat muscle activation patterns and changes in heading or among-wingbeat orientation might be due to any of three possibilities. First, because of the dependence of aerodynamically important variables on the preceding wingbeats, muscle activation patterns associated with turning cannot be evaluated on a per-wingbeat basis but must be analyzed as a sequence. This likely requires an experimental design with variation in the magnitude, speed and duration of the turns. Interrupting or disrupting turns in progress might also prove informative. Second, different flight muscles work together to generate the aerodynamic forces necessary to complete a turn. In this case, no individual muscle determines changes in roll or heading and therefore attempts to correlate activation patterns from individual muscles to overall changes in roll or heading are unlikely to succeed. Instead, the aerodynamic and neuromuscular control mechanisms employed by turning birds might be investigated with statistical methods suited for extracting information from several inter-related variables, such as a principal components analysis or construction of muscle synergies (e.g. d'Avella et al., 2003). The EMGs we were able to collect from the cockatoos include too few samples to be suitable for either of these approaches. Third, individual muscles may be linked to specific kinematic parameters such as wing rotation, extension and wingbeat amplitude that may themselves interact to generate both aerodynamic and inertial rotation. In this case, combining specific kinematic parameters to estimate aerodynamic torque and inertial reorientation might prove successful. In the companion paper to this study, we develop a detailed aerodynamic and inertial model for predicting changes in roll and show how individual muscles interact with different kinematic inputs to the model (Hedrick et al., 2007).

Inertial versus aerodynamic changes to roll orientation

We found evidence that both inertial and aerodynamic effects were important in determining changes in roll orientation, especially within a single wingbeat. This finding was not described in any prior studies of avian maneuvering flight and was not included in our initial hypotheses. Our measurements of roll angle through the wingbeat cycle revealed a complex pattern that included both within- and among-wingbeat variation (Fig. 8). A power spectrum analysis of the instantaneous roll angle (Fig. 8B) revealed the greatest signal strength at 3 Hz, slightly less than half-wingbeat frequency, and at 7.5 Hz, the birds' wingbeat frequency. However, these separate signals were unrelated, as the magnitude and direction of roll velocity in the higher frequency component were not significantly correlated with changes in roll over longer timescales. This lack of correlation suggests separate origins for the within- and among-wingbeat changes in roll orientation. Moreover, the roll angle we measured experimentally was not the roll angle of a discrete, rigid body. Instead, we measured the roll angle or orientation of the cockatoo's body, a relatively large mass linked to two smaller masses (the wings) that are actuated by muscles and oscillate about the body. Differences in the phase and magnitude of the wing oscillations likely generate asymmetric aerodynamic forces during maneuvers, but also have inertial consequences for body orientation that are independent of any aerodynamic forces they might generate. Changes in body orientation due to the inertial effects of asymmetric wing motion, such as the velocity differences noted by Warrick and Dial (Warrick and Dial, 1998), would occur primarily at wingbeat frequency. Our simplified model of inertial reorientation (Appendix 1) and simulation of a cockatoo flapping its left and right wings through different amplitudes demonstrated that the within-wingbeat changes in roll were, at least in part, the result of inertial forces. The asymmetric wing movements that cause inertial 'rocking' may also generate aerodynamic force asymmetries, but changes in roll due to these aerodynamic asymmetries would be in addition to inertial roll.

Because the moment of inertia of the cockatoos' wings differs between downstroke and upstroke, inertial effects may produce net changes in whole body roll orientation (see Appendix 1). However, we showed that these among-wingbeat changes must be smaller in magnitude than the within-wingbeat inertial effects. The predicted net change in orientation due to inertial effects ranged from 1° to 3° per wingbeat, but may be larger if both temporal and amplitude asymmetries are included. In either case, these net inertial changes to roll act in concert with aerodynamic asymmetries to produce the observed among-wingbeat changes in roll. Given the magnitude of measured among-wingbeat changes in roll, 13.9±11.0° (N=60), *versus* the expected inertial contribution of 1–3°, we conclude that aerodynamic effects were more important than inertial effects in determining among-wingbeat change in roll.

Roll versus yaw

Our tests of the relationship between roll angle, yaw rate and rate of change in heading in downstroke (see Results) demonstrated that the rate of change in heading was associated with roll angle, not yaw rate as might be expected in a yaw-based turn (Warrick et al., 1998). Thus, like pigeons, cockatoos used roll-based rather than yaw-based turns. However, yaw was

associated with turning, presumably to maintain the bird's orientation with respect to its flight path.

The cockatoos might also need to compensate for adverse yaw generated by changes in roll orientation. Adverse yaw, a yaw moment to the opposite side of the roll and a typical result of roll in fixed wing aircraft, occurs because increases in the lift generated by a wing are coincident with increases in drag on the same wing. Initiating a roll to the left by increasing the lift generated by the right wing also increases the drag from the right wing, resulting in a yaw moment to the right. However, birds and other flying animals generate both lift and thrust with their wings. Hence, an increase in lift could potentially be coupled with an increase in thrust rather than an increase in drag. Like roll, yaw angles measured on the body respond to internal forces generated by kinematic asymmetries in the wing stroke. Therefore, instantaneous aerodynamic effects such as adverse yaw cannot be quantified without a wingbeat kinematic and kinetic model that removes inertial effects from the instantaneous angular measurements. An examination of the lower frequency changes in yaw (Fig. 4) revealed only that roll and yaw change together through the wingbeat, but failed to clarify if one consistently led the other. Because the net changes in yaw over the course of a wingbeat were not in the adverse direction we concluded that the cockatoos generated a yaw moment into the turn to counter any adverse yaw on the time scale of a complete wingbeat.

Cockatoos versus pigeons

Most prior studies of avian maneuverability (Dial and Gatesy, 1993; Warrick and Dial, 1998; Warrick et al., 1998) used pigeons (*Columba livia*) rather than the cockatoos studied here. The cockatoos were somewhat smaller than typical pigeons (body mass of ~286 g *vs* ~350–400 g) and had a lower wing loading (~3.4 kg m^{-2} *vs* ~5.4 kg m^{-2}). These differences give the cockatoos greater steady-state gliding or intrinsic maneuverability, but it is not known how these differences might affect peak maneuvering performance in flapping flight (Warrick and Dial, 1998). We chose to work with the cockatoos because they rapidly learn to fly in various types of experimental apparatus. We taught the cockatoos to fly through the maneuvering course in approximately 30 min, whereas Warrick and Dial (Warrick and Dial, 1998) note that it took pigeons several weeks of training to learn a similar course. Additionally, aside from the specialized 'grippler' variety, pigeons fly poorly in wind tunnels, increasing the difficulty of linking steady state and maneuvering flight mechanics in that species (Rothe and Nachtigall, 1987). However, cockatoos and pigeons are phylogenetically distinct, likely diverging in the late Cretaceous (Ericson et al., 2006), and it may be that different bird clades employ different kinetic and neuromuscular mechanisms in turning. We believe that such a result would be a surprise, given the generally similar avian flight anatomy that is shared by these two species and was well established before the cockatoo and pigeon lineages diverged. Even so, this issue cannot be addressed by the limited scope of flight maneuvering studies performed to date.

The mode of turning used by the cockatoos in this study best fits the saltatory turning model (Warrick et al., 1998), with the birds apparently using small aerodynamic and net inertial torque asymmetries to establish a roll angle over several wingbeats. Our data do not support the alternative 'symmetric turning' mode, where roll orientation is established in a single wingbeat at the start of the turn and is constant thereafter. We reach somewhat different conclusions than the prior 3D kinematic study of pigeon turning (Warrick and Dial, 1998). However, these discrepancies likely reflect different analysis approaches rather than different mechanisms on the part of the birds. We found that within-wingbeat changes in roll angle were a combination of inertial and aerodynamic effects, where the inertial effects largely cancel over the course of a complete cycle but contribute a large portion of roll velocity at any point in time. We then separately analyzed the between-wingbeat changes in roll, for which aerodynamic forces are more important and inertial effects smaller. The among-wingbeat changes in roll orientation observed here for the cockatoos, which we assign primarily to asymmetric aerodynamic forces, were the result of roll accelerations of ~40 rad s^{-2}, measured at mid-downstroke. These accelerations were much smaller than those reported by Warrick and Dial (Warrick and Dial, 1998), who do not explicitly separate aerodynamic and inertial roll. However, separation of roll acceleration into inertial and aerodynamic components does show how small differences in pectoralis force such as those reported by Warrick et al. (Warrick et al., 1998) potentially give rise to both the small among-wingbeat roll accelerations reported here and the larger within-wingbeat roll accelerations and decelerations reported in Warrick and Dial (Warrick and Dial, 1998). Because inertial changes to orientation occur quickly, with four separate and opposing phases of rotational acceleration in every wingbeat, roll accelerations that include inertial and aerodynamic components will be large even in cases of modest asymmetries in wing arc or muscle force. Furthermore, inertia causes both roll acceleration and roll deceleration within a half stroke as the dominant wing first gains more and then loses more angular momentum than the other wing. Among-wingbeat aerodynamic and net inertial changes in orientation occur over the course of the complete wingbeat, leading to smaller instantaneous roll accelerations such as those reported here.

Appendix 1

Inertial reorientation

Consider the simple case of a bird with one wing flapping about a single axis at the shoulder, a system represented by two masses connected by a hinge joint. A torque produced by the pectoralis muscle at the joint will accelerate the wing as follows:

$$\dot{\omega}_{\text{wing}} = \frac{\tau}{I_{\text{wing}}}, \qquad \text{(A1)}$$

where $\dot{\omega}_{\text{wing}}$ is the angular acceleration of the wing, τ is the torque applied by the muscle, and I_{wing} the moment of inertia

of the wing. Acceleration of the wing gives rise to an increase in angular momentum, but because the system has not been subjected to any external forces, net angular momentum must remain 0:

$$I_{\text{body}}\omega_{\text{body}} - I_{\text{wing}}\omega_{\text{wing}} = 0\ , \qquad \text{(A2)}$$

where I_{body} is the moment of inertia of the bird's body about the shoulder joint and where ω_{body} and ω_{wing} are the angular velocities of the body and wing. If we assume that angular velocity is constant and is therefore the arc divided by cycle time, Eqn A2 becomes:

$$\beta_{\text{body}} = \frac{I_{\text{wing}}\beta_{\text{wing}}}{I_{\text{body}}}\ , \qquad \text{(A3)}$$

where β_{wing} is the arc that the wing moved through and β_{body} is the complementary change in the bird's body orientation. This equation gives the maximum change in roll of the body at the end of half a wingbeat cycle. For the bird to continue flapping it must complete the cycle, swinging its wing through an arc of $-\beta_{\text{wing}}$ and resulting in no net change in β_{body}:

$$\Delta\beta_{\text{body}} = \frac{I_{\text{wing}}\beta_{\text{wing}}}{I_{\text{body}}} - \frac{I_{\text{wing}}\beta_{\text{wing}}}{I_{\text{body}}} = 0\ . \qquad \text{(A4)}$$

However, in cases where the moment of inertia changes through time, β_{body} can undergo a net change. Consider two halves of a stroke cycle, one with the wing extended and one with the wing flexed:

$$\Delta\beta_{\text{body}} = \frac{I_{\text{Ewing}}\beta_{\text{wing}}}{I_{\text{body}}} - \frac{I_{\text{Fwing}}\beta_{\text{wing}}}{I_{\text{body}}}\ , \qquad \text{(A5)}$$

where I_{Ewing} and I_{Fwing} are the moments of inertia of the extended and flexed wing, respectively. Because all these formulations consider the effect of one wing, the net effect on the bird is the difference between the effects of the right and left wings.

We wish to thank the late Dr Russell Baudinette for facilitating this work at the University of Adelaide. Jayne Skinner and Craig McGowan also contributed enormously to the experiments; the work could not have been completed without their assistance. The manuscript was greatly improved by comments from Jim Usherwood and Sanjay Sane. The manuscript also greatly benefited from the comments of two anonymous referees. This project was funded by NSF IBN-0090265 to A.A.B.

References

Brown, R. H. J. (1953). The flight of birds. II. Wing function in relation to flight speed. *J. Exp. Biol.* **30**, 90-103.

Buchanan, K. L. and Evans, M. R. (2000). The effect of tail streamer length on aerodynamic performance in the barn swallow. *Behav. Ecol.* **11**, 228-238.

D'Avella, A., Saltiel, P. and Bizzi, E. (2003). Combinations of muscle synergies in the construction of a natural motor behavior. *Nat. Neurosci.* **6**, 300-308.

Dial, K. P. (1992a). Activity patterns of the wing muscles of the pigeon (*Columba livia*) during different modes of flight. *J. Exp. Biol.* **262**, 357-373.

Dial, K. P. (1992b). Avian forelimb muscles and nonsteady flight: Can birds fly without using the muscles in their wings? *Auk* **109**, 874-885.

Dial, K. P. and Gatesy, S. M. (1993). Neuromuscular control and kinematics of the wings and tail during maneuvering flight. *Am. Zool.* **33**, 5.

Ericson, P. G. P., Anderson, C. L., Britton, T., Elzanowski, A., Johansson, U. S., Källersjö, M., Ohlson, J. I., Parsons, T. J., Zuccon, D. and Mayr, G. (2006). Diversification of Neoaves: integration of molecular sequence data and fossils. *Biol. Lett.* **2**, 543-547.

Evans, M. R. and Thomas, A. L. (1992). The aerodynamic and mechanical effects of elongated tails in the scarlet-tufted malachite sunbird: Measuring the cost of a handicap. *Anim. Behav.* **43**, 337-347.

Frohlich, C. (1980). The physics of somersaulting and twisting. *Sci. Am.* **242**, 154-164.

Hatze, H. (1988). High-precision three-dimensional photogrammetric calibration and object space reconstruction using a modified DLT approach. *J. Biomech.* **21**, 533-538.

Hedrick, T. L., Usherwood, J. R. and Biewener, A. A. (2004). Wing inertia and whole body acceleration: an analysis of instantaneous aerodynamic force production in cockatiels (*Nymphicus hollandicus*) flying across a range of speeds. *J. Exp. Biol.* **207**, 1689-1702.

Hedrick, T. L., Usherwood, J. R. and Biewener, A. A. (2007). Low speed maneuvering flight of the rose-breasted cockatoo (*Eolophus roseicapillus*). II. Inertial and aerodynamic reorientation. *J. Exp. Biol.* **210**, 1912-1925.

Loeb, G. E. and Gans, C. (1986). *Electromyography for Experimentalists*. Chicago: The University of Chicago Press.

Maynard Smith, J. (1952). The importance of the nervous system in the evolution of animal flight. *Evolution* **6**, 127-129.

Norberg, U. M. (1981). Flight, morphology and the ecological niche in some birds and bats. *Symp. Zool. Soc. Lond.* **48**, 173-197.

Norberg, U. M. and Rayner, J. M. V. (1987). Ecological morphology and flight in bats (Mammalia; Chiroptera): wing adaptations, flight performance, foraging strategy and echolocation. *Philos. Trans. R. Soc. Lond. B Biol. Sci.* **316**, 335-427.

Pennycuick, C. J., Alerstam, T. and Hedenström, A. (1997). A new low-turbulence wind tunnel for bird flight experiments at Lund University, Sweden. *J. Exp. Biol.* **200**, 1441-1449.

Rayner, J. M. V. (1988). Form and function in avian flight. *Curr. Ornithol.* **5**, 1-66.

Rothe, H.-J. and Nachtigall, W. (1987). Pigeon flight in a wind tunnel. I. Aspects of wind tunnel design, training methods and flight behaviour of different pigeon races. *J. Comp. Physiol. B* **157**, 91-98.

Tobalske, B. W., Hedrick, T. L. and Biewener, A. A. (2003). Wing kinematics of avian flight across speeds. *J. Avian Biol.* **34**, 177-184.

Tucker, V. A. (1973). Bird metabolism during flight: evaluation of theory. *J. Exp. Biol.* **58**, 689-709.

Warrick, D. R. and Dial, K. P. (1998). Kinematic, aerodynamic and anatomical mechanisms in the slow, maneuvering flight of pigeons. *J. Exp. Biol.* **201**, 655-672.

Warrick, D. R., Dial, K. P. and Biewener, A. A. (1998). Asymmetrical force production in the maneuvering flight of pigeons. *Auk* **115**, 916-928.

Woltring, H. J. (1986). A FORTRAN package for generalized, cross-validatory spline smoothing and differentiation. *Adv. Eng. Software* **8**, 104-113.